Desalination and Water Treatment
www.deswater.com
1944-3994/1944-3986 © 2012 Desalination Publications. All rights reserved
doi: 10.1080/19443994.2012.705966

Taylor & Francis
Taylor & Francis Group

48 (2012) 390–403
October

CFD analysis of the fluid flow behavior in a reverse electrodialysis stack

Luigi Gurreri, Alessandro Tamburini, Andrea Cipollina, Giorgio Micale*

Dipartimento di Ingegneria Chimica, Gestionale, Informatica, Meccanica, Università di Palermo, viale delle Scienze (Ed.6), 90128 Palermo, Italy
Email: giorgiod.maria.micale@unipa.it

Received 13 May 2012; Accepted 20 June 2012

ABSTRACT

Salinity Gradient Power by Reverse Electrodialysis (SGP-RE) technology allows the production of electricity from the different chemical potentials of two differently concentrated salty solutions flowing in alternate channels suitably separated by selective ion exchange membranes. In SGP-RE, as well as in conventional ElectroDialysis (ED) technology, the process performance dramatically depends on the stack geometry and the internal fluid dynamics conditions: optimizing the system geometry in order to guarantee lower pressure drops (ΔP) and uniform flow rates distribution within the channels is a topic of primary importance. Although literature studies on Computational Fluid Dynamics (CFD) analysis and optimization of spacer-filled channels have been recently increasing in number and range of applications, only a few efforts have been focused on the analysis of the overall performance of the process. In particular, the proper attention should be devoted to verify whether the spacer geometry optimization really represents the main factor affecting the overall process performance. In the present work, realized within the EU-FP7 funded REAPower project, CFD simulations were carried out in order to assess the effects of different parameters on the global process efficiency, such as the choice of spacer material and morphology, and the optimization of feed and blowdown distribution systems. Spacer material and morphology can affect the fluid dynamics inside each channel. In particular, the appropriate choice of net spacer material can influence the slip/no-slip condition of the flow on the spacer wires, thus significantly affecting the channel fluid dynamics in terms of pressure drops. A *Unit Cell approach* was adopted to investigate the effect of the different choices on the fluid flow along the channel. Also, the possibility of choosing a porous *medium* to substitute the net spacer was theoretically addressed. Such investigation focused on the porosity and the fiber radius required to respect the process constrains of pressure drops and mechanical stability. On the other hand, the overall pressure drops of a SGP-RE or ED stack can be considered as resulting from different contributions: the pressure drop relevant to the feed distributor, the pressure drop inside the channel, and the pressure drop in the discharging collector. The choice of the optimal stack geometry is, therefore, strongly related to the need of both minimizing each of the above terms and obtaining the most uniform feed streams distribution among the stack channels. In order to investigate such aspects, simulations were performed on a simplified ideal planar stack with either 50 spacer-less or 50 spacer-filled channels. The effect of the distribution/collector channel

*Corresponding author.

Presented at the International Conference on Desalination for the Environment, Clean Water and Energy, European Desalination Society, 23–26 April 2012, Barcelona, Spain

thickness and geometry on single-channel flow rates and overall pressure drops in the system was analyzed and a significant influence of distributor layout and size on the overall process performance was found.

Keywords: CFD; Modeling; Stack design; Pressure drops; Spacer-filled channel

1. Introduction

In recent years, several research efforts have been devoted to find alternative renewable energies which could be sustainable and economically competitive. Renewable energies based on inexhaustible resources as sun and water are the most attractive. In this regard, the *salinity gradient power* (SGP) is a renewable energy form which can be drawn by the chemical potential difference between two different salt-concentrated aqueous solutions. It was estimated that the global potential power from the mixing of seawater and river water is 2.6 TW [1].

Reverse electrodialysis (RE) is a SGP technology based on the controlled mixing between two different concentrated solutions. This can be obtained by means of ionic exchange membranes. The consequent ions transport generates an electric potential difference which can be drawn as electric power [2].

The optimization of this technology is essential to guarantee its development and spreading. The EU-FP7 funded REAPower project fully addressed this issue by aiming at the development of a multiscale approach, which just starts from the Computational Fluid Dynamics (CFD) analysis of spacer-filled channel and fluid flow behavior within a SGP-RE stack.

The fluid flow features and conditions strongly affect the process performance. The pressure drops along the entire system (including the distributor, the spacer-filled channel, and the collector) should be minimized in order to reduce the pumping power. On the other hand, the driving force has to be maximized by keeping the concentration polarization as low as possible (e.g. by including a spacer within the channel). In addition, flow rates distribution within a stack of 100 up to 1,000 channels represents an issue which cannot be neglected [3,4]. All these aspects confirm the need to investigate the fluid flow of SGP-RE apparatuses by a powerful tool as the CFD.

Despite these considerations, to the authors knowledge, a very little attention has been paid to the CFD analysis of SGP-RE processes so far: only Dirkse et al. [5] addressed this topic by developing a model based on potential flow theory in order to predict the velocity and pressure field in flat-sheet geometries to be employed for SGP-RE applications. On the other hand, many works have been devoted to the CFD modeling of spacer-filled channels designed for other processes, such as: reverse osmosis, membrane distillation, ultra-filtration, etc. [6–13]. In accordance with these studies, the presence of the spacer significantly influences the fluid flow inside the channel in terms of pressure drops, concentration polarization, distribution of vortexes, recirculation zones, and shear stress.

Karode and Kumar [7] were the first adopting a CFD model to predict the fluid flow field in rectangular spacers filled channels for membrane modules. Their model was able to correctly predict the experimental dependence of the total drag coefficient on the Reynolds number. Moreover, for spacers with a low interfilament distance to filament diameter ratio, they stated that: (i) the fluid bulk flows parallel to the spacer wires and (ii) the pressure drop was mainly due to an abrupt change in the direction of the velocity vectors across the plane of spacer filaments intersection.

According to Ranade and Kumar [8], a spacer-filled channel can be considered as a set of connected periodic cells. They proposed to model via CFD one of these representative periodic cells (*Unit Cell approach*) in order to allow fine computational grid to be employed and small-scale flow structures to be consequently predicted. They quantified the different contributions of form and viscous drag to the total drag. Also, they investigated spacers with different cross-sections in order to minimize the form drag.

The same Unit Cell approach was adopted by Koutsou et al. [9] who performed direct numerical simulations of the flow within diamond spacer-filled channels. The simulation was carried out by setting the ratio of the distance between parallel filaments to the filament diameter (L/D) and the angle between the crossing filaments (β). The results showed that there are recirculation zones, which may trap the fluid and consequently affect concentration polarization effects. Also, they found that an increase of the L/D ratio and/or a decrease of the β angle lead the pressure drops along the channel to decrease. Finally, they stated that the presence of a spacer inside the channel causes maxima of time-averaged local wall shear stresses to be notably higher than those corresponding to empty channels as a confirmation of the increased mixing in the channel.

Li and Tung [13] deeply investigated the impact that the choice of different unit cells has on the CFD simulation of spacer-filled channels. They found that some unit cell types are suitable only for symmetric spacers, while may be unreliable for the case of asymmetric spacers. According to their findings, the most reliable unit cell is a domain periodic portion, where the filaments overlap at the center of its lateral faces, because only in this case the lateral areas can be judged as being equivalent. Finally, they investigated a full-scale module and stated that simulating a very low number of unit cells can be sufficient to predict with high accuracy the experimental pressure drop values of the full-scale module.

Most literature works addressing fluid dynamics aspects in spacer-filled channel mainly aim at finding the spacer allowing the best compromise between pressure drop reduction and polarization minimization. Nevertheless, there are many aspects which have not been taken into account yet.

- Spacers can be made of different materials: Spacer material characteristics influence the sliding of the fluid along the spacer wire surfaces thus likely modifying the channel fluid flow and the relevant pressure drops. This effect may be not negligible at low overall flow rates (corresponding to the laminar regime) as those typically encountered in SGP-RE channels.
- There are many commercially available porous media which couple a high open porosity with a high mixing promotion: the possibility to substitute a commercial spacer with one of these porous media should be addressed. In particular, a medium of fibers provides a very large number of locations for the membranes, thus assuming some "corrugated" aspect. For the case of ElectroDialysis and SGP-RE applications, this is likely to promote turbulence near their surfaces and consequently reduce concentration polarization phenomena [14].
- Although the contribution of the spacer geometry and/or the channel features to the process performance cannot be certainly neglected, a not sufficient attention has been paid to verify whether these are the main factors controlling the entire process. In this regard, according to some authors [5,15], the pressure losses in the manifolds and in the feed channel can be very larger than those recorded in the membrane-equipped-channel. Moreover, in SGP-RE applications the layout of the entire stack (distributor channels-collector) and the relevant flow rate distributions may affect the performance of the process.

The present study aims at filling these gaps in the literature by addressing each of these aspects for the case of a stack devoted to SGP-RE applications.

2. CFD modeling

2.1. Governing equations

The motion governing equations of a Newtonian and incompressible fluid are the continuity and momentum equations:

$$\vec{\nabla} \cdot \vec{u} = 0 \tag{1}$$

$$\rho \vec{u}\, \vec{\nabla} \cdot \vec{u} = -\ \vec{\nabla} p + \mu \nabla^2 \vec{u} \tag{2}$$

where u is the velocity, ρ is the density, μ is the dynamic viscosity, and p is the pressure. The fluid dynamics regime within the system under study in this work can be considered as being laminar at all the flow rates investigated [16]. As a consequence, no turbulence models have been employed and only laminar steady state simulations were carried out. Thus, the time-dependent term was not included in the momentum equation. Also, the fluid buoyancy was neglected.

In the present work, porous media filled channels were also investigated. In these cases, a source term corresponding to Darcy's generalized law was included in the momentum equation:

$$\vec{S}_{\mathrm{M}} = -\frac{\mu}{k}\vec{u} - k_{\mathrm{loss}}\frac{\rho}{2}u\vec{u} \tag{3}$$

where k is the permeability and k_{loss} is the loss coefficient which takes into account the possible deviations from the linear Darcy law for fluid flow with high Reynolds numbers. The linear term of this expression refers to viscous losses, while the quadratic term concerns inertial losses. Notably, the porous media were considered as being isotropic.

2.2. Numerical method

The finite volume code *Ansys-CFX 13* was employed to discretize and solve the former equations. The high resolution scheme was used for the discretization of the convective terms and shape functions were used to evaluate spatial derivatives for all the diffusion terms. A coupled algorithm was adopted for the pressure–velocity coupling.

A different number of iterations depending on flow rate values, system geometry, etc. were used for

the present steady state simulations. These numbers were chosen in order to guarantee that all the round mean square residuals settle at values lower than 10^{-6}.

The simulated fluid was pure water with $\rho = 997\,kg/m^3$ and $\mu = 8.899E{-}4\,Pa\,s$.

The present work will be divided in different sections according to its aim, i.e. addressing three different unexplored aspects concerning the fluid flow of the reverse electrodialysis process:

- assessing the effect of the spacer material on the pressure drops along the channel;
- evaluating whether a porous medium could substitute the most commonly adopted net spacers; and
- investigating an entire system aiming at addressing the effect of some parameters (distributor thickness, channels thickness, presence of a spacer, and layout configuration) on the SGP-RE process fluid dynamics.

Each section will present details on both numerical description and results discussion.

3. Effect of net spacers material

3.1. Spacer features

Two different double layer symmetric net spacer topologies were investigated: a commercial spacer made of woven wires and a corresponding ideal spacer made of overlapped filaments (Fig. 1). The diameter of each filament is 190 μm (the channel diameter is 380 μm), the distance between two subsequent coplanar filaments is 1.1 mm, the angle between two crossing filaments is 90˚, and the angles between the main liquid flow direction and the filaments are 45˚.

Notably, the size of these spacers was chosen according to that commonly adopted in small-scale electrodialysis plants.

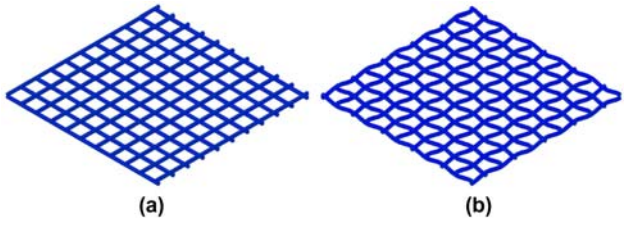

Fig. 1. Double layer net spacers sketch: (a) overlapped spacer 380 μm thick and (b) woven spacer 380 μm thick.

3.2. Unit Cell approach

The fluid flow analysis of the spacer-filled channels was performed by adopting the Unit Cell approach. According to this approach, the simulation of a periodic repetitive unit can be considered as being representative of the fluid flow within the entire spacer-filled channel, with the exceptions of the zones near the lateral walls. Several studies have demonstrated the soundness and the reliability of this approach [8,9,13]. Translational periodic boundary conditions were imposed along the main flow direction (*Z*-axis in Fig. 2) and along one of its perpendicular directions (*X*-axis). The membrane areas and the wires surfaces were simulated as walls. Either no-slip or free-slip conditions were imposed on the wires surfaces in order to assess the effect of the spacer material on the results (for full details see Section 3.3). A sketch of one of the adopted unit cell is depicted in Fig. 2.

According to the Unit Cell approach, a pressure gradient has to be imposed along the main flow direction in order to allow the fluid to move within the channel [13].

The two unit cells relevant to each spacer-filled channel were discretized by means of hybrid meshes mainly composed by hexahedral elements: because of the geometrical complexities due to the spacer wires, parallelepipeds were built around each filament and discretized with tetrahedrons while all the rest of the computational volume was discretized with mapped hexahedral elements. According to the literature, hexahedral grids lead to results being more reliable and closer to the experimental data [16–18]. Notably, all the meshes were finer in the proximities of domain walls (e.g. spacer wire surfaces).

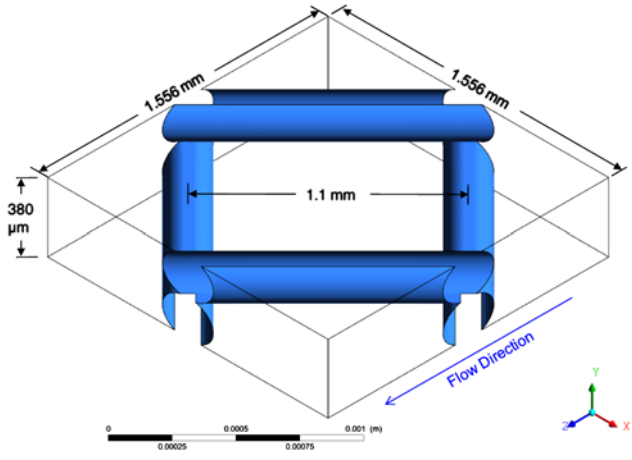

Fig. 2. Unit cell for the case of the 380 μm thick overlapped spacer.

A sensitivity analysis of the results dependence on the discretization degree was performed: both local and global quantities (e.g. the average velocity in the whole domain) were compared as a function of the number of computational elements for the case of the highest velocity investigated. As a result, the coarsest grid allowing results being "practically unaffected" (i.e. discrepancies of global quantities lower than 2%) by any grid dependence was found for all the three unit cells. The features of these grids are summarized in Table 1.

One of this grid dependence analyses is shown in Fig. 3 as an example.

3.3. Results and discussion

Different materials are used to produce commercial spacers (e.g. PET, PP, and PA). Materials with different characteristics may influence the system fluid flow patterns. As an example, completely hydrophobic and completely hydrophilic spacers offer a different resistance to the sliding of the water along the wire surfaces. Nevertheless, independently of the material constituting the spacer, the wire surfaces are very often defined as walls with no-slip boundary conditions in the literature [7,8,10,12]. Under turbulent conditions, the effect of this simplification may be considered as being small or even negligible. On the contrary, at the low flow rates corresponding to a laminar regime as those typically employed in SGP-RE channels, this influence cannot be passed over.

Table 1
Summary of the employed grids for the Unit Cell approach

Unit cell	Number of elements	% of volume discretized with hexahedral elements
380 μm woven spacer	~534,000	76.0%
380 μm overlapped spacer	~519,000	94.3%

In order to investigate the spacer material effect, the unit cells relevant to the two 380 μm spacer-filled channels (i.e. the woven and the overlapped one) were simulated by imposing either no-slip or free-slip boundary conditions on the filaments surfaces. These can be considered as the two opposite conditions at which different materials may lead.

Some different pressure drops were imposed and the corresponding flow rates were provided by the code. The corresponding results are shown in Fig. 4: the free-slip condition leads to lower pressure losses for both the two cases as expected because of the viscous stresses reduction. In particular, at a given flow rate, a large average discrepancy, calculated as $(\Delta P/l_{\text{no-slip}} - \Delta P/l_{\text{free-slip}})/\Delta P/L_{\text{no-slip}}$, can be observed for the two different conditions: for the case of the overlapped spacer it was about 42%, while it was about 46% for the case of the woven spacer.

Also, it can be observed that the pressure drops along the channel caused by the woven spacer are fairly higher than those relevant to the overlapped spacer: this average difference is of about 41 and 36% for no-slip and free-slip conditions, respectively.

According to these findings, it can be stated that the spacer material may affect the pressure drop slightly more than the geometric shape thus suggesting that the proper attention should be paid to the choice of the spacer material for SGP-RE applications. In particular, the adoption of hydrophobic materials, which intrinsically do not hold the water and reduce wall viscous stresses, should be preferable.

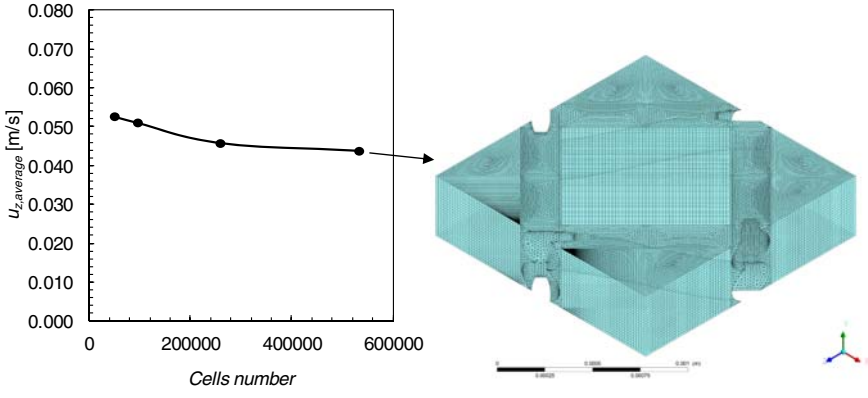

Fig. 3. Grid dependence analysis and the adopted mesh for the case of the 380 μm thick woven spacer.

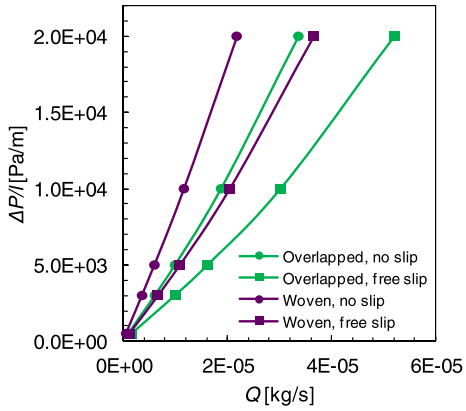

Fig. 4. Pressure drop per unit length in unit cell for overlapped and woven spacers both with free-slip and no-slip conditions on the filament surface. Notably, $Q = 1E{-}05$ kg/s in the unit cell corresponds to 38.7 ml/min within a channel 10 cm wide.

Fig. 4 shows that the relation between water flow rate and pressure drops is linear only at the smallest flow rates. Similarly, the drag coefficient (C_d) vs. Reynolds number (Re) curves (not reported here) show that C_d is proportional to Re^{-1} only up to a given flow rate. Despite this lack in linearity at high flow rates, the flow field regime is however laminar since the velocity vs. time trends did not show any chaotic fluctuation in the flow rate range investigated in the present work [16]. This nonlinear behavior is due to the spacer presence, which causes the flow field not to be auto-similar as the flow rates increases [16].

4. Porous spacer

A suitable porous medium filled channel would guarantee a good mixing, thus sensibly reducing concentration polarization phenomena. On the other hand, its structure allegedly would yield very large pressure drops. In this regard, CFD simulations of a channel filled with a purposely manufactured porous medium were carried out by Tamburini et al. [16]: results showed that the pressure drops along the channel were very larger than those relevant to net spacer filled channels, thus leading the authors to judge the porous medium as likely being unsuitable for SGP-RE processes.

As a consequence, this section is devoted to identify the characteristics that a porous medium must have to provide pressure drops along the channel comparable to those relevant to the formerly presented net spacers (see Section 3.1).

There are several analytical methods allowing to relate the microstructure of a porous medium with its permeability. The permeability of a fibrous medium depends on different factors:

- fiber size, e.g. the fibers radius a;
- fiber concentration, usually expressed as solid volumetric fraction or as porosity ε (clearly $\phi = 1 - \varepsilon$); and
- fiber arrangement.

At a given fiber arrangement, the relation between permeability and the other two variables can be expressed as follows:

$$\frac{k}{a^2} = f(\phi) \tag{4}$$

In accordance with the most commonly adopted theoretical approach [19–26], a porous medium can be ideally considered as a matrix of rods in order to explicit the function $f(\phi)$.

Porous media made of random fibrous structure were already investigated as possible fillers of channels devoted to SGP-RE processes [16]. As a consequence, theoretical relations being suitable and valid for this kind of porous media were adopted in the following. In particular, two different analytical models were employed: the Jackson and James model [19] and the model by Tomadakis and Robertson [20].

According to the first one, the random medium permeability is considered as being equivalent to the permeability of a cubical lattice made of the same material. This results in the following expression for the dimensionless permeability:

$$\frac{k}{a^2} = \frac{3}{20\phi}\left(-\ln\phi - 0.931 + o(\ln\phi)^{-1}\right) \tag{5}$$

Conversely, Tomadakis and Robertson [20] developed an analytical model based on electrical conduction principles aiming at predicting the permeability of porous media made of random fiber structures. The corresponding relation for the dimensionless permeability was:

$$\frac{k}{a^2} = \frac{\varepsilon}{8(\ln\varepsilon)^2}\,\frac{\left(\varepsilon - \varepsilon_p\right)^{\alpha+2}}{\left(1-\varepsilon_p\right)^{\alpha}\left[(\alpha+1)\varepsilon - \varepsilon_p\right]^2} \tag{6}$$

where ε is the medium porosity, ε_p is the percolation threshold, and α is a constant. For three-directional random overlapping fiber structures, $\varepsilon_p = 0.037$ and $\alpha = 0.661$. Full details can be found in the relevant work [20].

Eqs. (5) and (6) are plotted in Fig. 5. As it can be seen, these provide the similar dimensionless

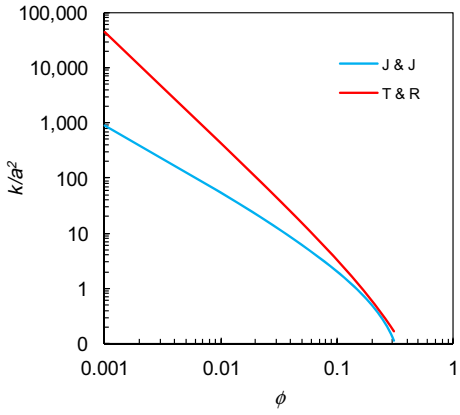

Fig. 5. Dimensionless permeability as a function of solid volume fraction.

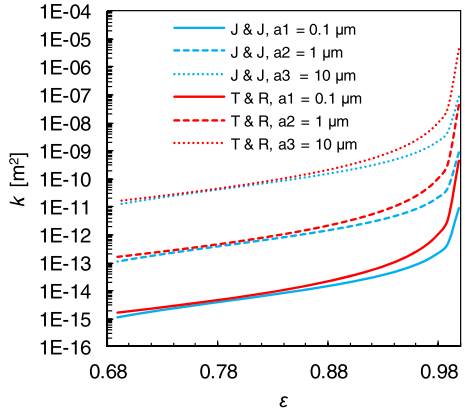

Fig. 6. Permeability as a function of the porosity for three fiber radius values.

permeability for solid volume fraction higher than 0.2, while for ϕ lower than 0.1, the lower the ϕ value, the larger the values of dimensionless permeability obtained by the relation by Tomadakis and Robertson [20] with respect to the Jackson and James equation [19].

In order to find the characteristics of a fiber structure porous medium providing pressure drops comparable to those relevant to a net spacer, three different fiber radius values (i.e. $a_1 = 0.1\,\mu m$, $a_2 = 1\,\mu m$, and $a_3 = 10\,\mu m$) were investigated. The relevant permeability as a function of the porosity is shown in Fig. 6 for the case of the two former equations.

These values were adopted along with a given flow rate $Q = 5 \times 10^{-6}\,kg/s$ and a cross-section $A = 0.38 \times 1.556\,mm^2$ (equal to the one used in the unit cell CFD simulations) to calculate the corresponding pressure losses by Darcy's law. Fig. 7 shows the obtained pressure drop values. Notably, the pressure drops relevant to the two "completely hydrophilic" spacer (i.e. no-slip condition) filled channels (the woven and the overlapped spacer) are also reported for comparison purposes.

Results show that the lower the fiber radius, the higher the porosity required to provide pressure drops along the channel ΔP_{ch} similar to those relevant to the spacer. As an example, a fiber radius equal to $10\,\mu m$ would require a porosity higher than 95%, while a porous medium made of $1\,\mu m$ fibers would require values of ε larger than 99%. A low fiber radius along with a very large porosity are likely to be requirements incompatible with the mechanical stability of the membrane-equipped-channels. On the other hand, ΔP_{ch} comparable with the net spacers may be obtained by employing porous media made of very large fiber radius whose size should be about one

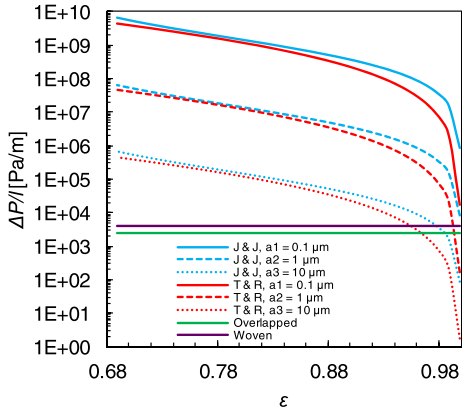

Fig. 7. Pressure drop as a function of the porosity for three fiber sizes, for a flow rate $Q = 5 \times 10^{-6}$ kg/s, and a cross-section $A = 0.38 \times 1.556\,mm^2$.

hundreds microns, thus assuming the same features of a common wire made spacer.

Summarizing, these considerations suggest that a "feasible" porous medium made of small fibers (whose size is lower than typical spacer wire size) allegedly provides pressure drops along the channel very larger than those relevant to a typical spacer, thus allegedly being unsuitable for SGP-RE applications.

5. Simplified entire stack

5.1. Geometrical features and numerical details

In order to evaluate the contributions of manifolds on the overall pressure loss as well as the effect of stack layout and geometry on the flow rate distribution within the channels, an ideal 50-channels stack was devised: it is a "not-cylindrical" stack (distributor

and collector are rectangular channel) with only a computational cell along the *X*-axis, so that it can be somewhat considered as a planar-like (2D) stack.

This numerical simplification of the real 3D geometry is adopted in view of its large computational savings: the simulation of an entire 3D stack would require very large computational resources, especially for the case of channels filled with a spacer. However, this simplification can be considered reasonable as the fluid dynamics along the unconsidered direction (*X*-axis) is not crucial for the pressure drop contributions estimation and for the flow rates distribution assessment.

Therefore, only a sheet (along the *X*-axis) of the entire stack was modeled by using a single computational cell along this direction. The channels length was equal to 10 cm. Conversely, two different channel thicknesses were investigated: either 100 μm or 200 μm in accordance with the idea of designing stacks as compact as possible. The distance between two subsequent channels was set to 300 μm for the case of 100 μm channel, while it was 400 μm for the case of the 200 μm channels. Three different distributor widths s were simulated: $s_1 = 0.2$ mm, $s_2 = 0.5$ mm, or $s_3 = 1.0$ mm. Full details of the 2D stack are shown in Fig. 8.

Both the empty and spacer-filled channels were investigated: in particular, for the case of the 200 μm channels, the effect relevant to the presence of the woven spacer was addressed. As a consequence, an ideal woven spacer 200 μm thick, similar to the 380 μm one previously presented, was employed in this section. A Unit Cell approach along with a relevant grid dependence analysis was preliminary performed for this spacer. A hybrid mesh of 1,200,000 elements was found to be more than sufficient to avoid any dependence of results on discretization degree.

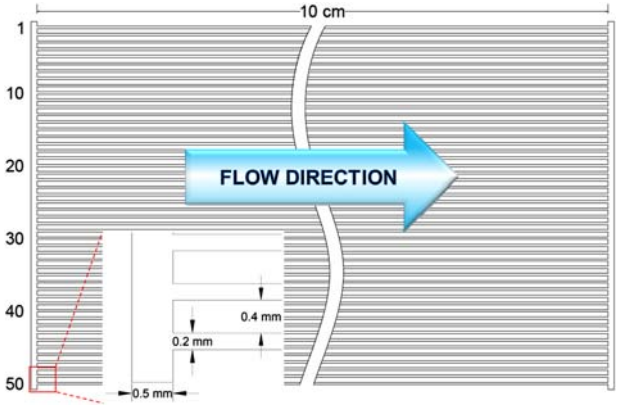

Fig. 8. 2D geometry stack with 50 channels 200 μm thick and distributor and collector width equal to 0.5 mm.

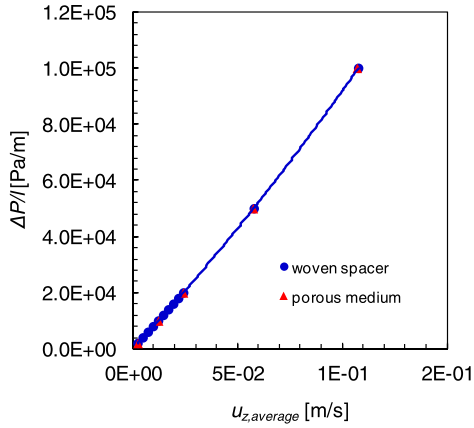

Fig. 9. Pressure drop per unit length along the unit cell for: woven spacer 200 μm thick and equivalent porous medium.

However, it is not possible to simulate the effect of a spacer in a 2D geometry by considering only a sheet of the spacer. This problem was tackled by filling the channels with a fictitious porous medium able to provide pressure drops along the channel identical to those provided by the presence of the corresponding spacer. More precisely, first the pressure drops along the 200 μm thick spacer-filled channel were evaluated as a function of the flow rates by means of the Unit Cell approach and a relevant $\Delta P/l$ vs. average u_z (velocity component along the main flow direction) graph was provided (Fig. 9). Then, these results were fitted by a second-order equation composed of two parameters (Fig. 9): these two parameters are considered as the k and k_{loss} (see Eq. (3)) of the corresponding fictitious porous medium.

As far as boundary conditions are concerned, a uniform normal velocity corresponding to the flow rates investigated (see Table 2) was set as inlet condition, a pressure equal to the atmospheric one was set as outlet condition, symmetry boundary conditions were imposed on the surfaces perpendicular to the neglected direction. All other stack surfaces were defined as walls along with no-slip boundary conditions.

Two different inlet–outlet configurations were investigated:

- a configuration A with a single inlet and a single outlet and
- a configuration B with two inlets and two outlets.

These two configurations are depicted in Fig. 10.

Notably, a summary of the different features/conditions investigated for the case of this simplified entire stack are reported in Table 2.

Table 2
Summary of the investigated variables

Distributor/ Collector width (mm)	Channels thickness (μm)		Feed configuration	Flow rate	
s_1	0.2	w_1 spacer less	100	A (single inlet and single outlet)	$Q_{over\text{-}1}$	4.00E−06 kg/s[a] 240.7 ml/min[b]
s_2	0.5	w_2 spacer less and spacer filled	200	B (double inlet and double outlet)	$Q_{over\text{-}2}$	2.00E−05 kg/s[a] 1203.6 ml/min[b]
s_3	1.0				$Q_{over\text{-}3}$	4.00E−05 kg/s[a] 2407.2 ml/min[b]

[a]Flow rate value within the 2D stack.
[b]The corresponding flow rates within a stack 10 cm wide.

A grid dependence analysis was performed also for the case of the simplified entire stack and it is not presented here for brevity. The chosen grids range from a minimum of 534,000 to a maximum of 1,365,000 computational elements because of the different geometrical features under investigation. It could appear as surprising that the entire stack requires a grid as fine as those relevant to a singular unit cell. Actually, the channels constituting the stack are either empty or filled with the fictitious porous medium, there are no spacers thus resulting in low computational requirements.

5.2. Results and discussion

The geometry of the entire stack may significantly affect the SGP-RE process performance. As a matter of fact several factors influencing the net power production depend on the stack geometrical features: concentration polarization phenomena, driving force across the membranes, short-cut currents, channels electrical resistance, total pumping power, and flow rate distribution are the most crucial among these factors.

In this section, the dependence of *some fluid flow aspects* (i.e. the flow rate distributions within the channels, the overall pressure drop, and its different contributions within the stack) on *some of the stack geometrical feature*s (i.e. the distributor, collector and channel size, the presence of the spacer, and the feed configuration at three different feed flow rates) is investigated by carrying out a number of CFD simulations on the simplified 50 channels entire stack.

All the variables and their relevant values investigated are summarized in Table. 2: notably simulations encompass all the possible combinations of these variable values.

5.2.1. Flow rate distribution

The flow rate value within each channel clearly depends on the pressure difference between the distributor and the collector. Thus, the flow rates distribution along the channels can be inferred by the former pressure difference as a function of the *Y*-coordinate.

In this regard, two lines parallel to the *Y*-axis were placed in the middle of both the distributor and the collector as it can be seen in Fig. 11. As an example, the behavior of the total pressure along these two lines is shown in Fig. 12 for the simulation case relevant to flow rate $Q_{over\text{-}2} = 2E{-}5\,kg/s$, distributor/collector width $s_2 = 0.5\,mm$, and spacer-less channel thickness $w_2 = 200\,\mu m$. The corresponding collector–

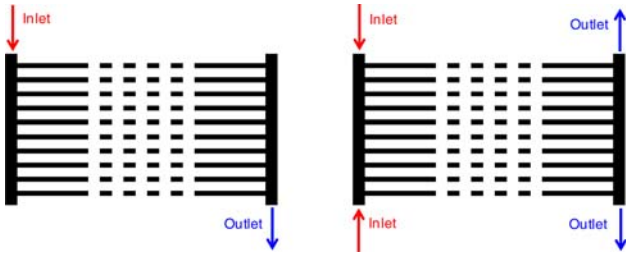

Fig. 10. The two different inlet–outlet configurations tested: (left) single inlet–single outlet (conf. A); (right) double inlet–double outlet (conf. B).

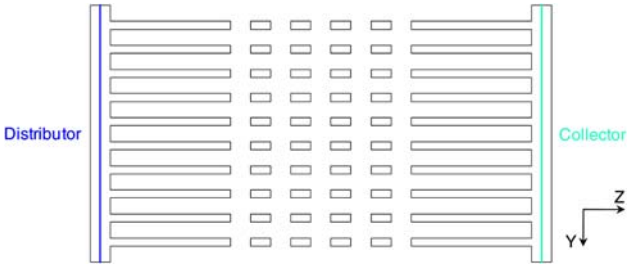

Fig. 11. Indication of the lines parallel to the *Y*-axis placed in the center of the distributor and collector.

distributor pressure differences trend (as a function of the *Y*-coordinate), which can be inferred from the figure, suggests that the flow rate distribution along the channels is not uniform. As a matter of fact, the flow rate shows a minimum which is always relevant to the central channel for the case of the configuration B, while it can vary its position as a function of collector/distributor width and overall flow rate for the case of configuration A.

From Fig. 12, it appears that the total pressure curves relevant to the configuration B are perfectly symmetric, thus suggesting that this configuration leads to a symmetric flow rates distribution along the channels. And also in accordance with the geometrical symmetry of this configuration it is not surprising.

Flow rates distribution as a function of all the investigated parameters is provided in Figs. 13 and 14: in particular, the flow rates relevant to some channels only (the 1st, 13th, 26th, 38th, and 50th) are presented.

In Fig. 13, the dependence of flow rates distribution on channel features and stack configuration is shown. The flow rates distribution relevant to the spacer-less 100 μm channel is the most uniform. For the case of the 200 μm channels, in general the flow rate distribution is poorer and a difference between the spacer-filled and the spacer-less channel is

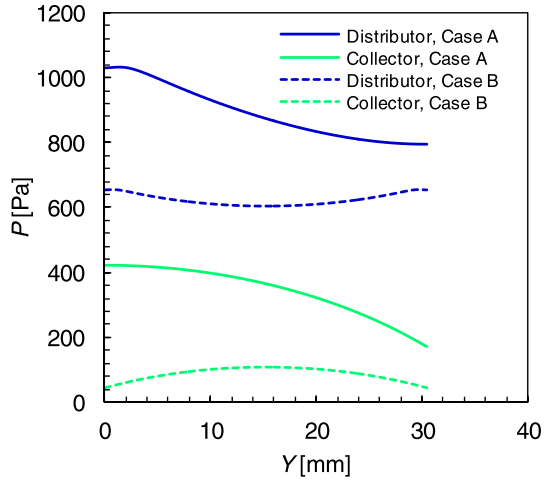

Fig. 12. Total pressure along two lines parallel to the *Y*-axis and placed in the middle of the distributor and the collector, respectively. Simulation case with flow rate $Q_{over\text{-}2} = 2E{-}5$ kg/s, distributor/collector width $s_2 = 0.5$ mm, and spacer-less channels thickness $w_2 = 200$ μm.

highlighted. In particular, the presence of a spacer leads to an enhancement of the flow rates distribution uniformity with respect to the corresponding spacer-less channels. This indicates that the higher the pressure drops along the channels (spacer-less 100 μm channel provides the highest pressure drops), the more homogeneous the corresponding flow rates distribution. In fact, the pressure difference between the distributor and the collector is the driving force to the water flow inside each channel. Therefore, with reference to Fig. 12, the larger the distance between the two pressure curves (the one relevant to the collector and that relevant to the distributor), the more uniform the distribution of the "driving force" along the stack and thus the more uniform the flow rates distribution.

The effect of the distributor/collector width and of total flow rate on the flow rates distribution is presented in Fig. 14 for the case of the spacer-filled channels 200 μm thick.

As regards the effect of the distributor/collector width *s*, the figure shows that a higher *s* corresponding to lower pressure losses along the entire stack results into a better flow rates distribution for both the configurations. As far as the pressure drops along the distributor/collector reduces because of an increase of their width, the corresponding total pressure vs. *Y*-coordinate (Fig. 12) curves tend to flatten, thus resulting into more homogeneous pressure differences along *Y* (i.e. more uniform flow rates distribution).

As far as the influence of the overall flow rate on its distribution degree along the various channels is concerned, results of Fig. 14 show that an increase of

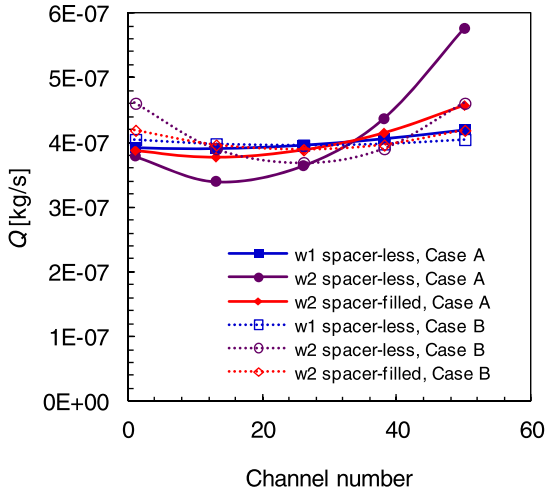

Fig. 13. Flow rates distribution in some channels (1st, 13th, 26th, 38th, and 50th) for the case of flow rate $Q_{over\text{-}2} = 2E{-}5\,kg/s$ and distributor/collector width $s_2 = 0.5\,mm$. Notably, $Q = 4E{-}07\,kg/s$ in the 2D stack corresponds to 24.07 ml/min within a stack 10 cm wide.

the Q_{over} yields a worse flow rate distribution along the channels, especially for the case of the configuration A, while a very little influence was observed for the symmetric configuration. However, it is worth noting that the effect of the overall flow fate on its distribution along the channels is not significant with respect to the effects relevant to distributor/collector width and channel features, thus suggesting that investigations should focus on these last two effects.

As previously anticipated and as also observed in Figs. 13 and 14, the employment of the configuration B always leads to a symmetric and more uniform flow rates distribution thanks to its intrinsic geometrical symmetry.

On summarizing, it can be concluded that the flow rate will be distributed more uniformly in stacks characterized by higher pressure drops along the channels (lower channels thickness and presence of spacers) or lower pressure drops along the distributor and collector (configuration B, higher distributor and collector width).

Notably, the flow rates distribution may affect the total SGP-RE process performance: in this regard, the results provided by the present CFD simulation were used as input data for a process simulator [4]. In accordance with the results obtained by this process simulator, a bad flow rates distribution leads to a reduction of the power density, especially at low overall flow rates [4].

5.2.2. Pressure losses along the entire stack

The contribution of the distributor to the overall pressure losses ΔP_{over} was addressed. For the case of the configuration A, this ΔP_{distr} was calculated as:

$$\Delta P_{distr} = P_{inlet} - P_{50} \tag{7}$$

where P_{inlet} is the total pressure at the inlet surface and P_{50} is the pressure just afterward the 50th channel.

Similarly, for the case of the configuration B:

$$\Delta P_{distr} = P_{inlet} - P_{min} \tag{8}$$

where P_{min} is the minimum total pressure in the distributor, it is achieved midway between the 25th and the 26th channels.

Relevant results and comparison are provided in Fig. 15. ΔP_{distr} is linearly dependent on the overall flow rate on the basis of the laminar regime and it reduces as the distributor width increases as expected.

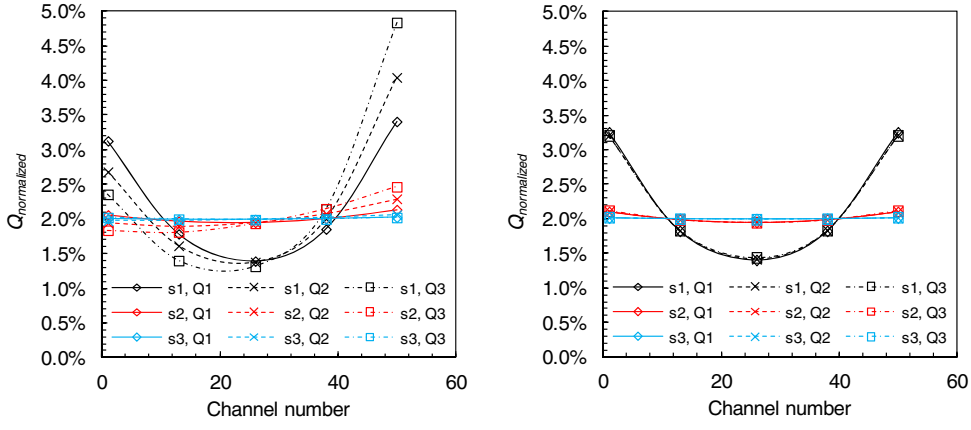

Fig. 14. Flow rates distribution in some spacer-filled channels 200 μm thick (1st, 13th, 26th, 38th, and 50th). Left: configuration A and right: configuration B.

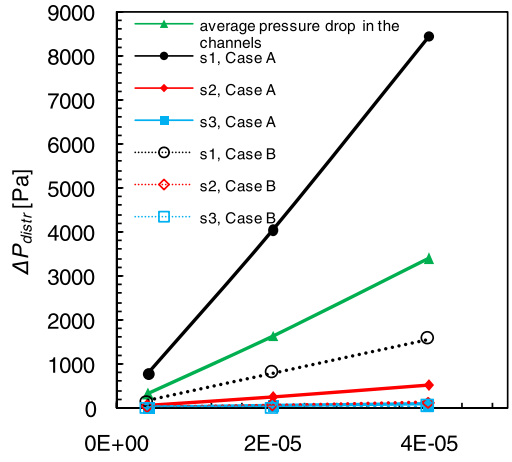

Fig. 15. Pressure losses along the distributor and average pressure drop along the spacer-filled channel. Notably, $Q_{over} = 1E{-}06$ kg/s in the 2D stack corresponds to 60.18 ml/min within a stack 10 cm wide.

Fig. 15 shows also that in some cases, ΔP_{distr} is of the same order of magnitude of the average pressure drop along the channel ΔP_{ch} (calculated as the arithmetic average of the pressure drop along the various channels), thus suggesting that both the contributions are important and should be taken into account. In particular, for the case of the stack with the smallest distributor width s_1 (i.e. $s_1 = 0.2$ mm) and the configuration A, ΔP_{distr} is about twice as ΔP_{ch}, while they are practically the same for the configuration B. As a difference, in all the other cases ΔP_{ch} corresponds to the main contribution to the overall pressure drops. Also, the configuration B always leads to ΔP_{distr} being lower than those relevant to the configuration A.

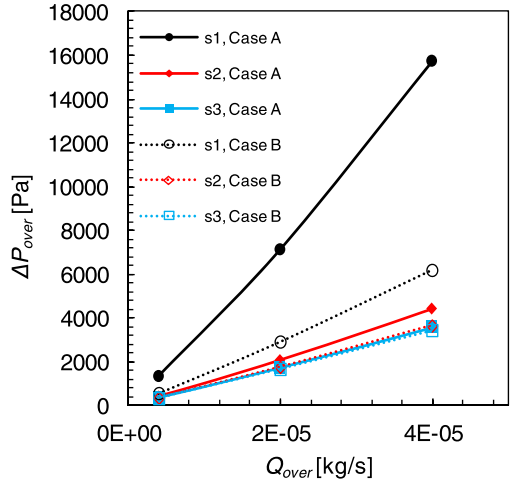

Fig. 16. Overall total pressure drops along the entire stack for the case of spacer-filled channels. Notably, $Q_{over} = 1E{-}06$ kg/s in the 2D stack corresponds to 60.18 ml/min within a stack 10 cm wide.

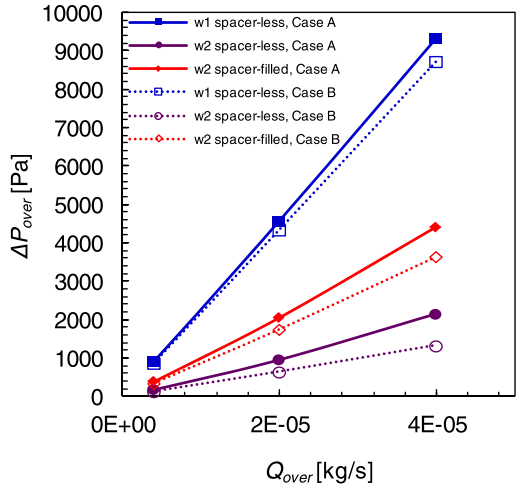

Fig. 17. Overall pressure drops along the entire stack at a given distributor/collector width ($s_2 = 0.5$ mm). $Q_{over} = 1E{-}06$ kg/s in the 2D stack corresponds to 60.18 ml/min within a stack 10 cm wide.

A linear dependence of the overall total pressure ΔP_{over} (calculated as $P_{inlet} - P_{outlet}$) on the overall flow rate can be observed in Fig. 16. The trends corresponding to the distributor width s_2 and s_3 are similar, since for these two cases, the main contribution to ΔP_{over} is due to the pressure losses along the channel ΔP_{ch}. Conversely, the case relevant to the distributor thickness s_1 exhibits a larger ΔP_{over} because of the main contribution due to the distributor.

Fig. 17 shows that the channel geometrical features (i.e. thickness and spacer presence) also significantly affect ΔP_{over}. In particular, both a decrease of the channel thickness and the presence of a spacer lead ΔP_{over} to increase as expected. Clearly, at a given distributor/collector thickness, the choice of channel geometrical features resulting in larger ΔP_{ch} causes the distributor contribution of ΔP_{over} to be less important.

6. Conclusions

Analysis and CFD simulations of a simplified stack including spacer-filled channels for reverse electrodialysis applications were carried out in order to assess the influence of different aspects on the fluid flow performance of the process.

In particular, three different aims were pursued:

- assessing the effect of the spacer material on the pressure drops along the channel;
- evaluating whether a fiber structure porous medium may substitute the most commonly adopted net spacers;

- addressing the effect of some parameters (distributor thickness, channels thickness, presence of a spacer, and layout configuration) on the fluid dynamics of a simplified SGP-RE system.

Results show that the spacer geometry optimization may not be the main factor affecting the overall process efficiency.

At a small scale, the spacer material can affect the sliding conditions of the fluid on the spacer filaments thus modifying the flow field along the channel and the relevant pressure drops. In particular, a suitable perfectly hydrophobic material able to avoid any friction between the flowing water and the spacer wires would provide a significant reduction (about 40%) of the pressure drops along the channel with respect to a spacer made of a perfectly hydrophilic material providing water to filaments no-slip conditions.

As far as the possibility of adopting a suitable porous medium instead of a net spacer is concerned, a theoretical analysis of porous media characteristics was performed. In particular, two different theoretical approaches (based on the simplification of considering the porous medium as a rods matrix) were adopted in order to assess the porosity and the fiber radius that a porous medium should have to provide ΔP_{ch} similar to those caused by typical net spacers. A low fiber radius along with a very large porosity would lead to ΔP_{ch} similar to those provided by the spacers, but they are likely to be two slight compatible properties. On the other hand, large fiber radius may also be suitable to accomplish the desired task, but the fiber radius size should be so large that the porous medium shape would become the same of a commercial net spacer. These findings suggest that a feasible porous medium made of small fibers (whose size is lower than typical spacer wire size) allegedly provides pressure drops along the channel very larger than those relevant to a typical net spacer, thus likely being unsuitable for SGP-RE applications.

At a larger scale, fluid flow performance depends not only on the channels characteristics, but also on stack geometry and layout. The dependence of some fluid flow aspects (i.e. the flow rate distributions within the channels, the overall pressure drop, and local pressure drops ΔP_{distr} and ΔP_{ch}) on some features of the stack (i.e. different distributor, collector and channel size, spacer presence, feed configuration, and overall feed flow rate) was investigated by carrying out a number of CFD simulations on a simplified 50 channels entire stack. Results indicate that all the parameters considered can affect the stack fluid dynamics.

- A more homogeneous distribution of liquid flow rates can be obtained by: (i) increasing the pressure drops along the channel (i.e. decreasing channels thickness and/or adding a spacer), (ii) decreasing hydraulic losses in the distributor (i.e. decreasing distributor/collector width), and (iii) reducing the total flow rate.
- An analysis of the overall pressure losses along the stack has shown that a fluid flow optimization of a SGP-RE apparatus must not focus on channel features only. In fact, in some cases the pressure drops along the distributor were found to be larger or of the same order of magnitude of the average pressure drop along the channel.

The adoption of a symmetric feeding configuration along with an increasing number of inlets is suggested to provide better flow rates distribution and lower pressure losses, although it is intrinsically more complex and expensive from a construction point of view.

Finally, it is worth noting that all the results presented in this work have been employed as input data in a process simulator [4] aiming at developing an integrated approach able to allow an overall optimization of SGP-RE processes.

Acknowledgments

This work has been performed within the REAPower (Reverse Electro dialysis Alternative Power production) project, funded by the EU-FP7 programme (Project Number: 256736)—website www.reapower.eu.

Notations

A	—	cross-section (m^2)
a	—	fiber radius (m)
C_d	—	drag coefficient (–)
d_h	—	hydraulic diameter (m)
k	—	permeability (m^2)
k_{loss}	—	empirical loss coefficient (m^{-1})
p	—	pressure (Pa)
P	—	total pressure (Pa)
P_{50}	—	total pressure just afterward the 50th channel (Pa)
P_{inlet}	—	total pressure at the inlet (Pa)
P_{min}	—	minimum total pressure in the distributor (Pa)
P_{outlet}	—	total pressure at the outlet (Pa)
Q	—	mass flow rate (kg s^{-1})
Q_{over}	—	overall flow rate in the simplified entire stack (kg s^{-1})
Re	—	Reynolds number (–)

s — distributor/collector width (mm)
S_M — source term for porous domain (kg m^{-2} s^{-2})
u — velocity (m s^{-1})
u_z — velocity component along the main flow direction (m s^{-1})
w — channels thickness (μm)
$\Delta P/l$ — total pressure drop per unit length (Pa m^{-1})
ΔP_{distr} — total pressure drop in distributor (Pa)
ΔP_{over} — overall total pressure drop in the stack (Pa)

Greek letters

α — constant in dimensionless permeability expression (–)
ε — volume porosity (–)
ε_p — percolation threshold (–)
μ — dynamic viscosity (Pa s)
ρ — density (kg m^{-3})
ϕ — solid volume fraction (–)

References

[1] G.L. Wick, W.R. Schmitt, Prospects for renewable energy from sea, Mar. Technol. Soc. J. 11 (1977) 16–21.
[2] R.E. Lacey, Energy by reverse electrodialysis, Ocean Eng. 7 (1980) 1–47.
[3] J. Veerman, M. Saakes, S.J. Metz, G.J. Harmsen, Reverse electrodialysis: A validated process model for design and optimization, Chem. Eng. J. 166 (2011) 256–268.
[4] M. Tedesco, A. Cipollina, A. Tamburini, W. van Baak, G. Micale, Modelling the Reverse ElectroDialysis process with seawater and concentrated brines. Paper accepted for publication on Desalination & Water Treatment, (2012), doi: 10.1080/19443994.2012.699355.
[5] M.H. Dirkse, W.K.P. van Loon, J.W. Post, J. Veerman, J.D. Stigter, G.P.A. Bot, Extending potential flow modelling of flat-sheet geometries as applied in membrane-based systems, J. Membr. Sci. 325 (2008) 537–545.
[6] A.R. Da Costa, A.G. Fane, C.J.D. Fell, A.C.M. Franken, Optimal channel spacer design for ultra-filtration, J. Membr. Sci. 62 (1991) 275–291.
[7] S.K. Karode, A. Kumar, Flow visualization through spacer filled channels by computational fluid dynamics I. Pressure drop and shear rate calculations for flat sheet geometry, J. Membr. Sci. 193 (2001) 69–84.
[8] V.V. Ranade, A. Kumar, Fluid dynamics of spacer filled rectangular and curvilinear channels, J. Membr. Sci. 271 (2006) 1–15.
[9] C.P. Koutsou, S.G. Yiantsios, A.J. Karabelas, Direct numerical simulation of flow in spacer-filled channels: Effect of spacer geometrical characteristics, J. Membr. Sci. 291 (2007) 53–69.
[10] J.L.C. Santos, V. Geraldes, S. Velizarov, J.G. Crespo, Investigation of flow patterns and mass transfer in membrane module channels filled with flow-aligned spacers using computational fluid dynamics (CFD), J. Membr. Sci. 305 (2007) 103–117.
[11] M. Shakaib, S.M.F. Hasani, M. Mahmood, Study on the effects of spacer geometry in membrane feed channels using three-dimensional computational flow modeling, J. Membr. Sci. 297 (2007) 74–89.
[12] S. Wardeh, H.P. Morvan, CFD simulations of flow and concentration polarization in spacer-filled channels for application to water desalination, Chem. Eng. Res. Des. 86 (2008) 1107–1116.
[13] Yu-Ling Li., Kuo-Lun Tung, CFD simulation of fluid flow through spacer-filled membrane module: Selecting suitable cell types for periodic boundary conditions, Desalination 233 (2008) 351–358.
[14] H. Strathmann, Electrodialysis. A mature technology with a multitude of new applications, Desalination 264 (2010) 268–288.
[15] J. Veerman, M. Saakes, S.J. Metz, G.J. Harmsen, Reverse electrodialysis: Performance of a stack with 50 cells on the mixing of sea and river water, J. Membr. Sci. 327 (2009) 136–144.
[16] A. Tamburini, G. La Barbera, A. Cipollina, M. Ciofalo, G. Micale, CFD simulation of channels for direct and reverse electrodialysis, Paper accepted for publication on Desalination & Water Treatment, (2012), doi: 10.1080/19443994.2012.705084.
[17] D. Molyneux, N. Bose, Escort tug at large yaw angle: Comparison of CFD predictions with experimental data, of the, International Journal of Small Craft Technology—Royal Institution of Naval Architects Transactions Part B 150 (2008) 41–60.
[18] H.I. Oguntade, G.E. Andrews, A. Burns, D. Ingham, M. Pourkashanian, CFD predictions of single row film cooling with inclined holes: influence of hole outlet geometry, Proceedings of the ASME Turbo Expo 4 (2010) 1371–1385.
[19] G.W. Jackson, D.F. James, The permeability of fibrous porous media, Canadian Journal of Chemical Engineering 64(3) (1986) 364–374.
[20] M.M. Tomadakis, J.T. Robertson, Viscous permeability of random fiber structures: Comparison of electrical and diffusional estimates with experimental and analytical results, Journal of Composite Materials 39(2) (2005) 163–188.
[21] I. Langmuir, Report of smokes and filters, Part IV of a report for the Office of Scientific Research and Development (OSRD), No. 865, Ser. No. 353, Filtration of aerosols and the development of filter materials, by W. H. Rodebush et al., September 4, 1942.
[22] E.M. Sparrow, A.L. Loeffler, Jr. Longitudinal laminar flow between cylinders arranged in regular array, AlChE J. 5 (1959) 325–330.
[23] J.E. Drummond, M.I. Tahir, Laminar viscous flow through regular arrays of parallel solid cylinders, Int. J. Multiphase Flow 10 (1984) 515–540.
[24] J. Happel, Viscous flow relative to arrays of cylinders, AIChE J. 5 (1959) 174–177.
[25] A.S. Sangani, A. Acrivos, Slow flow past periodic arrays of cylinders with application to heat transfer, Int. J. Multiphase Flow 8 (1982) 193–206.
[26] L. Spielman, S.L. Goren, Model for predicting pressure drop and filtration efficiency in fibrous media, Envir. Sci. Tech. 2 (1968) 279–287.